Quantifying the contribution of somatosensory afferent types and changes therein to pain sensitivity using transcutaneous optogenetic stimulation in behaving mice

Yu-Feng Xie[1], Christopher Dedek[1,2], Steven A. Prescott[1-3]*

[1]Neurosciences and Mental Health, The Hospital for Sick Children, Toronto, ON, Canada

[2]Institute of Biomedical Engineering, University of Toronto, Toronto, ON, Canada

[3]Department of Physiology, University of Toronto, Toronto, ON, Canada

*To whom correspondence should be addressed:

Steven A. Prescott, steve.prescott@utoronto.ca

Acknowledgements: We thank Jason Jeong for technical assistance and Stéphanie Ratté for feedback on the manuscript. This work was supported by a Foundation Grant from the Canadian Institutes of Health Research (FDN167276).

Declaration of interests: CD and SAP have filed a US patent (US 2024/0099652) on RAMalgo and have equity in Robotic Algometry Inc.

Author contributions: The project was conceived by CD and SAP. Experiments were carried out by YFX with assistance from CD. Data were analyzed by YFX with assistance from CD and SAP. SAP supervised all research. SAP produced the final manuscript with input from YFX and CD.

ABSTRACT

Optogenetics provides an unprecedented opportunity to delineate how different somatosensory afferents contribute to sensation, including pain. By expressing channelrhodopsin-2 (ChR2) in certain afferents, those afferents can be selectively activated by transcutaneous photostimuli applied to behaving mice. Despite the great care taken to precisely target expression of ChR2, imprecise photostimulation has hindered quantitative behavioral testing. Here, using a robot to reproducibly photostimulate behaving mice and precisely measure their paw withdrawal, we show that selectively activating nociceptors with ramped photostimuli evokes faster withdrawal than co-activating nociceptive and non-nociceptive afferents, consistent with gate control. We also show that inflammation-induced hyperexcitability in nociceptors is sufficient to increase pain sensitivity. Electrophysiological testing confirmed that inflammation increases nociceptor excitability without affecting phototransduction. Data further suggest that withdrawal latency depends on the number of nociceptors activated rather than how strongly each nociceptor is activated. Consistent with changes described in nociceptor somata, the behavioral consequences of peripherally blocking different voltage-gated sodium (Na_V) channels showed that nociceptor axons normally rely on $Na_V1.8$ but upregulate $Na_V1.7$ after inflammation, with important clinical implications for drug efficacy. Collectively, these results demonstrate the utility of optogenetic pain testing when reproducibly delivered and strategically designed photostimuli are used.

SIGNIFICANCE STATEMENT

Transcutaneous optogenetic stimulation was first applied to behaving mice to explore the neural basis for pain over a decade ago. Despite great care taken to control which afferents express optogenetic actuators, the sensitivity of such testing has been hindered by crude photostimulation methods and imprecise response measurement. Here, we demonstrate highly quantitative optogenetic pain testing using robotic stimulation and withdrawal detection. By comparing paw withdrawal to equivalent nociceptor activation with and without activation of non-nociceptive afferents, we demonstrate the antinociceptive effect of the latter input. We also demonstrate increased pain sensitivity due to inflammation-induced hyperexcitability in nociceptors and the associated change in Na_V isoform expression. We also show that withdrawal from ramped optogenetic stimulation reflects how many nociceptors are recruited.

INTRODUCTION

Optogenetics has revolutionized neuroscience by enabling specific neurons to be activated or inhibited using light (1). Specificity is achieved by targeting expression of light-sensitive actuators like ChR2 to genetically defined cell types, often using additional factors to refine expression (2-5). Less attention has been paid to targeting light but spatially precise photostimulation using optrodes (6) or multiphoton excitation (7) has enabled phototagging (8), efficient circuit mapping (9), and other applications that require control over the strength or pattern of neuronal activation. Photostimuli are typically applied as pulses which, if sufficiently strong and brief, evoke one spike per pulse (10). This allows neuron firing rate to be controlled by the photostimulus pulse rate, but it comes at the expense of evoking unnaturally synchronized spiking across activated neurons. Synchrony can be mitigated by adjusting photostimulus kinetics (11), and non-pulsed photostimuli have been used to study network resonance (12) and axon excitability (11), but these are exceptions to the near ubiquitous use of pulses. New optogenetic applications promise to emerge from improvements in photostimulus delivery and strategic photostimulus design.

Understanding of somatosensory processing especially stands to benefit from such improvements. Diverse somatosensory afferent types exist (13) but how they contribute to sensation remains contentious in part because natural stimuli tend to co-activate many afferents (14, 15). For instance, if mechanoreceptor activation reduces the pain driven by co-activated nociceptors (16), then mechanical allodynia could reflect reduced mechanoreceptor and/or increased nociceptor activation; resolving the contribution of each type of change (which likely differs between chronic pain etiologies) requires selective silencing of mechanoreceptors during painful mechanical stimulation, selective (e.g. optogenetic) activation of nociceptors, or similar experiments.

Optogenetics has already been applied along the entire somatosensory neuraxis (17, 18), including at the earliest stages of sensory transduction (19). Cutaneous afferents can be photostimulated non-invasively through the skin but spatiotemporal targeting of transcutaneous photostimuli has been crude. Past studies measuring withdrawal from transcutaneous optogenetic stimuli have relied exclusively on pulses (20-34), mostly applied by handheld fiber optic cables. Uncontrolled variability in photostimulation (35) and imprecise response measurement limit one's ability to resolve behavioral changes. This prompted us to develop a robot, RAMalgo, to reproducibly deliver optogenetic (and other) stimuli and precisely measure paw withdrawal (35).

Using RAMalgo to deliver ramped optogenetic stimuli to asynchronously activate select afferents in behaving mice, we demonstrate here that co-activating nociceptive and non-nociceptive afferents evokes slower withdrawal than exclusively activating nociceptors, consistent with gate control theory. We also demonstrate that inflammation-induced hyperexcitablity in nociceptors is sufficient to increase pain sensitivity, and that withdrawal latency depends on how readily nociceptors are activated by ramped optogenetic stimulation. By selectively blocking $Na_V1.8$ or $Na_V1.7$ channels in nociceptive axon terminals of naïve and inflamed mice, we also show that inflammation shifts the relative contribution of these Na_V isoforms to axon excitability. These results show that optogenetic pain testing can be far more quantitative than past studies would suggest.

RESULTS

To minimize stress due to handing (36), mice were transferred from their home cage in clear plastic tubes that are placed upright on the platform and slid into an opaque cubicle for testing (**Fig. 1A**). Mice were viewed from below by video. The stimulator, which is mounted on motorized actuators, was aimed by joystick for this study but autonomous aiming using AI is also possible (35); in either case, the experimenter remains far from the mice to avoid stressing them. Once the stimulator was aimed at the target paw, the red LED was illuminated to monitor movement based on changes in reflectance of red light off the paw (**Fig. 1B**). If the paw remained immobile during the user-defined prestimulus period, the blue LED was automatically illuminated. Photostimulus intensity was ramped up over 15 seconds because this (i) avoids the unnaturally synchronized spiking (see Introduction) and (ii) requires fewer trials to find threshold than titrating pulse amplitude (35). Photostimulation was applied to a spot 3.5 mm in diameter (**Fig. 1B top inset**). Withdrawal latency was measured from the red reflectance signal (**Fig. 1B**). A typical response to ramped photostimulation in a $Na_V1.8$-ChR2 mouse is shown in **Video 1** for comparison with a ChR2-negative mouse, which does not respond to equivalent stimulation (**Video 2**). Stimulation terminates automatically upon paw withdrawal and all data (including video) and metadata (date, time, stimulus parameters, etc.) were recorded to computer.

Withdrawal evoked by nociceptor activation is delayed by co-activating non-nociceptive afferents

To explore effects of activating different afferent types, we compared paw withdrawal evoked by equivalent optogenetic ramps applied to Nav1.8-ChR2 mice (which express ChR2 selectively in

nociceptors) and advillin-ChR2 mice (which express ChR2 in all afferents). Natural stimuli co-activate multiple afferent types (see Introduction) but cell-to-cell variations in transduction complicate efforts to control co-activation. For our experiments, all afferent types were activated via ChR2 and ChR2 expression was controlled by the same promoter in both mouse lines, thus enabling equivalent nociceptive input to be evoked with and without concurrent non-nociceptive input.

Withdrawal latency in $Na_V1.8$-ChR2 mice (1.926 $\pm$ 0.309 s, mean $\pm$ SEM) was significantly shorter than in advillin-ChR2 mice (4.614 $\pm$ 0.742 s) (**Fig. 1C**, T_{23} = -2.83, p = 0.009, unpaired t-test), meaning non-nociceptive input inhibits nociceptive input, consistent with gate control theory (16). If non-nociceptive afferents produced a purely inhibitory signal, then selectively activating them should not evoke withdrawal. To test this, we co-injected $Na_V1.8$- and $Na_V1.7$-specific blockers (PF-24 and PF-71, respectively) into the target paw of advillin-ChR2 mice to silence nociceptors before repeating optogenetic testing; $Na_V1.8$ and $Na_V1.7$ are both expressed preferentially in nociceptors (37, 38). This manipulation did not prevent withdrawal, but it did delay it by 2.853 $\pm$ 0.744 s (**Fig. 1C**, T_6 = -3.836, p = 0.009, paired t-test). This suggests that non-nociceptive afferents convey a mixed signal that can evoke withdrawal even if (some of) those afferents also inhibit the signal arriving from nociceptors, although nociceptors may not have been fully silenced. Beyond using optogenetics to control which afferents are activated, these results demonstrate the value of controlling how strongly those afferents are activated while precisely (yet efficiently) measuring the behavioral consequences.

Changes in optogenetically evoked withdrawal reveal hyperexcitability in nociceptor axons

Using $Na_V1.8$-ChR2 mice to focus on nociceptors, we compared optogenetic responses before and after inflammation caused by injecting complete Freund's adjuvant (CFA) into the target paw (**Videos 1** and **3** show responses in the same mouse before and after CFA, respectively). We found a significant interaction between treatment (saline vs CFA) and time (baseline vs. post-injection) ($F_{1,24}$ = 10.914, p = 0.003, two-way repeated measures ANOVA). Withdrawal latency differed significantly between CFA and saline conditions post-injection (p = 0.010, Student-Neuman-Keuls test) but not at baseline (p = 0.56). Withdrawal latency dropped significantly after CFA (**Fig. 2A left**, p < 0.001) whereas it increased slightly after saline (**Fig. 2A right**, p = 0.18). Based on within-mouse measurements, the 0.873 $\pm$ 0.212 s reduction after CFA differed significantly from the 0.519 $\pm$ 0.291 s increase after saline (**Fig. 2B**, T_{24} = -3.304, p = 0.003, unpaired t-test), revealing a large

effect of inflammation (Hedges' g = 1.54). Withdrawal latency at baseline did not differ significantly between males (2.278 ± 0.250 s, n = 18) and females (2.310 ± 0.382, n = 8) (T_{24} = -0.071, p = 0.94, unpaired t-test), nor did the reduction in latency caused by CFA differ significantly between males (0.808 ± 0.256 s, n = 14) and females (1.024 ± 0.408, n = 6) (T_{18} = -0.46, p = 0.65).

By activating only nociceptors, our testing isolated the behavioral consequences of inflammatory changes in nociceptors. Furthermore, because optogenetic stimulation bypasses natural transduction, our results exclude effects of inflammation on mechanical or thermal transduction, and instead highlight the behavioral consequences of nociceptor hyperexcitability. Specifically, our results show that inflammation-induced hyperexcitability in nociceptor axons is sufficient to increase pain sensitivity. This assumes ChR2 is not affected by inflammation (see below). These data do not exclude effects of inflammation on transduction, or effects of inflammation on other neuron types; both sorts of changes occur (see Discussion) but neither contribute to the heightened pain sensitivity reported here, allowing one to start parsing out such contributions.

Somatic excitability changes measured in vitro parallel axon changes inferred from behavior

To confirm that CFA increases nociceptor excitability without altering ChR2 expression or function, we electrophysiologically tested small-diameter ChR2-positive neurons harvested from control and inflamed (CFA-injected) mice. All recordings were conducted 2-8 hours after dissociation to avoid changes induced by culturing (11, 39). Neurons from inflamed mice (henceforth labeled "inflamed" neurons) were excited by weaker current injection and fired more vigorously than control neurons (**Fig. 3A**). Rheobase (i.e. the weakest current required to evoke a spike) in control neurons (14.5, 6 – 28 pA; median, interquartile range [IQR]) was higher than in inflamed neurons (4, 2 – 8.75 pA) (**Fig. 3B,** U_{27} = 36, p = 0.003, Mann-Whitney U test). Evoked firing rates revealed a significant interaction between stimulus intensity and condition (**Fig. 3C**, $F_{6,168}$ = 4.834, p < 0.001, two-way repeated measures ANOVA). Because rheobase was lower after inflammation and because we incremented stimulus intensity as multiples of rheobase, weaker stimuli were applied to inflamed neurons than to control neurons, which means even stronger effects of inflammation would have been seen by matching absolute stimulus intensities across conditions. The difference in evoked firing rate was at least partly due to the higher proportion of transient spiking neurons (i.e. unable to ever fire >2 spikes) relative to repetitive spiking neurons in control vs. inflamed conditions (**Fig. 3C inset**, χ^2 = 4.55, p = 0.033). Several other metrics were unchanged between

control to inflamed neurons: Resting membrane potential (-64.1 ± 2.5 mV vs -61.6 ± 1.8 mV, T_{27} = -0.833, p = 0.412), input resistance (2.29 ± 0.27 MΩ vs 2.35 ± 0.22 MΩ, T_{27} = -0.164, p = 0.871), and capacitance (15.45 ± 1.05 pF vs 14.90 ± 0.93 pF, T_{27} = 0.399, p = 0.693). These results demonstrate that inflammation increased the somatic excitability of nociceptors without affecting passive membrane properties.

Other changes (in active membrane properties) were evident by comparing the spike waveform in control and inflamed neurons (**Fig. 3D**). Spike threshold in control neurons (-38.1 ± 1.4 mV) was significantly more depolarized (i.e. less negative) than in inflamed neurons (-43.6 ± 1.6 mV) (**Fig. 3E**, T_{27} = 2.58, p = 0.016, unpaired t-test), which translated to a significant difference in spike height (86.25, 84 – 89 mV vs 91, 90.125 – 96.25 mV; U_{27} = 57, p = 0.038). Conversely, spike width in control neurons (2.775, 2.15 – 3.6 ms) was greater than in inflamed neurons (1.6, 1.413 – 1.975 ms) (**Fig. 3F**, U_{27} = 39, p = 0.004). Spike rise time in control neurons (2.4, 2.2 – 2.7 ms) was also greater than in inflamed neurons (2.0, 1.9 – 2.2 ms) (**Fig. 3G**, U_{27} = 42.5, p = 0.007). These changes, which have been reported previously (40), reflect a shift in the dominant sodium channel isoform from $Na_V1.8$ in control neurons to $Na_V1.7$ in inflamed neurons (39), which has notable implications (see Fig. 5).

Hyperexcitability increases optogenetically evoked spiking consistent with behavioral changes

Next, we checked if inflammation affects ChR2 function or expression. Voltage clamp recordings of the current evoked by different intensities of blue light applied as 1 s-long steps exhibited no differences in ChR2 gating between control and inflamed neurons but suggested a reduction in ChR2 expression (**Fig. 4A**). The ChR2 current evoked by 156 mW/mm^2 blue light in control neurons (24.5, 24 – 26 pA) was slightly larger than in inflamed neurons (17, 14.25 – 25.25 pA), but the difference did not reach significance (**Fig. 4B**, U_{27} = 61, p = 0.057). The modest reduction in ChR2 current did not offset the large increase in excitability in inflamed neurons according to optogenetically evoked spiking (see below).

Figure 4C illustrates sample responses to 15 s-long ramps of blue light. Kinetics match the ramps used for behavioral testing but the intensity of light reaching the target cannot be directly compared between in vitro and in vivo conditions, and nor can somatic and axonal excitability be directly compared. Nevertheless, latency to the first optogenetically evoked spike in control neurons (10.085, 0.785 – 15 s) was much longer than in inflamed neurons (0.940, 0.489 – 4.330 s)

(**Fig. 4D**, U_{27} = 63, p = 0.068). A subset of neurons did not respond with any spikes and were treated as having a latency of 15 s (i.e. the duration of the ramp). By measuring in voltage clamp the ChR2 current evoked in the same neuron to an equivalent photostimulus ramp, threshold ChR2 current was identified as the ChR2 current at the time of the first spike (see arrows on Fig. 4C). Threshold ChR2 current was significantly higher in control neurons (26, 7 – 36 pA) than in inflamed neurons (6.5, 3.5 – 9.275 pA) (**Fig. 4E**, U_{27} = 42.5, p = 0.007). As expected, each neuron's rheobase (i.e. injected current threshold) and ChR2 current threshold were similar (T_{13} = -1.155, p = 0.269 for control neurons and T_{14} = -0.821, p = 0.425 for inflamed neurons; paired t-tests). Fewer spikes were evoked in control neurons (1.75, 0 – 12 spikes) than in inflamed neurons (10, 1.625 – 48.25 spikes), but this difference did not reach significance (**Fig. 4F**, U_{27} = 65, p = 0.082). Interestingly, neurons identified as transient spiking (based on their response to current injection, see above) were significantly less likely to respond with any spikes to the optogenetic ramp (**Fig. 4F inset**, χ^2 = 7.03, p = 0.008). This is consistent with transient spiking neurons requiring abrupt depolarization to initiate spikes (41, 42); optogenetic ramps (unlike pulses) do not cause rapid enough depolarization to evoke spikes in most transient spiking neurons, which is notable since transient spiking neurons are less common after inflammation (see above).

To compare optogenetically evoked nociceptor spiking with optogenetically evoked paw withdrawal, consider that 60% (9 of 15) of inflamed cells were activated before withdrawal occurred in inflamed mice (1.472 s) whereas only 36% (5 of 14) of control cells were activated before withdrawal occurred in saline-injected mice (2.616 s). This suggests that inflamed cells, because of their heightened excitability, were recruited by weaker stimulation, thus triggering withdrawal at shorter latency. By comparison, despite a near-significant difference in the total number of spikes evoked by the optogenetic ramp in each condition, if the count is restricted to spikes occurring *before* the average withdrawal latency in each condition, few spikes occur in control or inflamed neurons (0, 0 – 2 spikes vs 2, 0 – 4) (U_{27} = 72.5, p = 0.14). From this, we surmise that it is the number of activated neurons that dictate when withdrawal is initiated, since most activated neurons each contribute only one spike before withdrawal occurs. Published data on responses to short (100 ms) optogenetic pulses provide additional context (35): Withdrawal from strong pulses occurred in as little as 20 ms but withdrawal to just-threshold pulses took as long as 500 ms. Since optogenetic ramps approach the threshold amplitude slowly, one should consider stimulus amplitude 500 ms before the observed response (based on the 500 ms latency for just-

threshold pulses). For the optogenetic ramps reported here, approximately 30% of neurons were activated 500 ms before the withdrawal latency in each condition, suggesting enough control neurons were recruited ~2 s after the start of the optogenetic ramp (2.616 – 0.5 = 2.116 s) whereas inflamed neurons required half as long to be sufficiently recruited (1.472 – 0.5 = 0.972 s), implying they required half as much stimulation because of their heightened excitability. These calculations are speculative but provide a valuable framework to guide future experiments.

Nociceptor axons experience the same shift in Na_V subunit contribution as somata

We showed previously that nociceptors rely on $Na_V1.8$ channels under normal conditions but that $Na_V1.7$ channels become more important after inflammation (39), consistent with spike waveform changes described in Figure 3D-G. Extrapolating from those data, we predicted that blocking $Na_V1.8$ (with PF-24) would delay paw withdrawal in control mice but not in inflamed mice, whereas blocking $Na_V1.7$ (with PF-71) would delay withdrawal in inflamed mice but not in control mice. In other words, the analgesic efficacy of PF-24 should decrease after inflammation whereas the efficacy of PF-71 should increase. Either drug was injected into the paw at the stimulation site to modulate axon excitability while measuring effects on withdrawal from optogenetic stimulation.

Figure 5 reports the change in withdrawal latency produced by injecting drug or vehicle (saline-diluted DMSO) into control or inflamed mice. Vehicle produced a modest reduction in withdrawal latency in control mice (0.583, -0.845 – 0.217 s) and inflamed mice (0.147, -0.275 – 0.225 s); the effect did not differ between groups (U_{21} = 34, p = 0.15, Mann-Whitney U test) and data were therefore pooled to give a median latency change of -0.290, -0.722 – 0.239 s against which to compare drug effects. As predicted, PF-24 significantly increased withdrawal latency by 6.871, 3.676 – 8.096 s in control mice (U_{27} = 1, p < 0.001; Hedges' g = 3.53) while insignificantly increasing withdrawal latency by 0.239, -0.073 – 0.552 s in inflamed mice (U_{25} = 24, p = 0.14; Hedges' g = 0.49). Conversely, PF-71 insignificantly increased withdrawal latency by 0.039, -0.564 – 0.624 s in control mice (U_{29} = 70, p = 0.33; Hedges' g = 0.54) but significantly increased it by 0.417, -0.133 – 3.066 s in inflamed mice (U_{29} = 40, p = 0.020; Hedges' g = 1.19). Effect sizes (quantified as Hedges' g values) showed that blocking either Na_V isoform delayed withdrawal in each condition, but blocking $Na_V1.8$ had ~7× greater effect in control mice (3.53/0.49 = 7.20) whereas blocking $Na_V1.7$ had ~2× greater effect in inflamed mice (1.19/0.54 = 2.20). These results confirm that nociceptor axon terminals experience the same inflammation-induced shift in Na_V expression as somata.

DISCUSSION

We applied transcutaneous optogenetic stimulation to behaving mice to explore how different afferent types contribute to nocifensive behavior, including how changes in afferent excitability modulate that behavior. Using ramped optogenetic stimulation while efficiently and sensitively measuring withdrawal latency, we showed that co-activating non-nociceptive afferents delays the withdrawal evoked by activating nociceptors (**Fig. 1**). We also found that inflammation-induced hyperexcitability in nociceptors increases pain sensitivity (**Fig. 2**). Electrophysiological testing in vitro confirmed that nociceptor excitability is increased by inflammation (**Fig. 3**) and that this hyperexcitability (rather than increased ChR2 current) increases responsivity to optogenetic stimulation (**Fig. 4**); expedited recruitment of hyperexcitable nociceptors likely explains why inflamed mice withdraw faster from ramped optogenetic stimuli. Our results also demonstrate that nociceptor axons normally rely on $Na_V1.8$, but $Na_V1.7$ is upregulated after inflammation (**Fig. 5**).

Pain behavior testing is notoriously irreproducible (43) but improved methods can change this. Optogenetics allows for exquisite control of *which* neurons are activated, but extra effort is required to control the strength and pattern of their activation. And so too must the behavioral consequences be accurately measured. Robotic stimulation and response measurement offer dramatic improvements over the status quo (35). Stable stimulation also affords the opportunity to apply prolonged stimuli, including ramps. We used photostimulus ramps for several reasons. First, ramps enable reliable determination of threshold with just a few trials; by comparison, pulses must be repeated at several intensities to plot an input-output curve (34) or otherwise pinpoint threshold (e.g. with an up-down method (44)). Second, ramp-evoked responses reflect changes in excitability more sensitively than pulse-evoked responses insofar as ramps tend not to activate transient spiking neurons (see Fig. 4F); this is reminiscent of work showing that electrical pulses are not a sensitive means to measure pain sensitivity (45). Third, ramping photostimulus intensity avoids the grossly unnatural spike synchrony associated with pulses, which is important for somatosensation (46). Ramped stimulation necessitates accurate measurement of withdrawal latency, but this is straightforward with our reflectance-based method (which is as accurate but far simpler and more cost-effective than high-speed videography). Thus, strategically designed photostimulus waveforms applied reproducibly with the appropriate technology provide new opportunities for reproducible, quantitative optogenetic pain testing.

Many molecular changes are induced by inflammation (47-49). The number of co-occurring changes

and the variety of neuron types affected make it difficult to pinpoint which changes in which neurons contribute to altered pain sensitivity. Based on our demonstration that activity in non-nociceptive afferents modulates the withdrawal driven by nociceptor activation (see Fig. 1C), we focussed on selective nociceptor activation in later experiments. Because we selectively activated nociceptors, the inflammation-induced increase in pain sensitivity reported in Figure 2 must be due to changes in nociceptors. Furthermore, since optogenetic activation bypasses thermal and mechanical transduction, the altered pain sensitivity must be due to heightened excitability. Our results do not mean transduction steps are not affected by inflammation, or that altered transduction or other changes in other cell types do not impact the pain evoked by other stimuli; instead, our data show that inflammation-induced hyperexcitability in nociceptors is sufficient to increase pain sensitivity. This may seem obvious based on correlational evidence (that inflammation increases both excitability and pain sensitivity) and evidence for necessity (that reversing hyperexcitability reduces pain sensitivity) but we are unaware of past evidence for sufficiency.

Our conclusion that inflammation-induced changes in cutaneous axon excitability mediate an increase in pain sensitivity is supported by the effects of subtype-selective Na_V inhibitors injected into the paw. Extrapolating from past experiments on somatic excitability (39), we predicted that pain sensitivity in control mice depends mostly on $Na_V1.8$, whereas pain sensitivity in inflamed mice depends mostly on $Na_V1.7$. Such knowledge is obviously important for choosing the best drug for a given pain condition. Inferring which ion channel to target based on an observed excitability change is, however, complicated by the fact similar excitability changes can arise from distinct molecular changes (50-52). Matters are further complicated by certain changes being unique to axons (53, 54), which risks them being overlooked in somatic recordings, but so too might somatic changes not generalize to axons. In the case of Na_V isoforms, both compartments experience the same inflammation-induced shift from $Na_V1.8$ to $Na_V1.7$. Beyond testing if a drug target on nociceptors changes, optogenetic testing can also help determine via which neuron type a drug modulates behavior, if, for example, the target is present on >1 type of neuron, especially if those neuron types are co-activated by natural stimuli. Many other experiments are conceivable.

Overall, these results demonstrate the utility of optogenetic pain testing, especially to dissect the contribution of different types of afferents to sensation. The opportunities are enhanced by technology like RAMalgo that can reproducibly stimulate and accurately measure withdrawal, and by strategically designing stimulus waveforms to optimize the sensitivity and efficiency of testing.

MATERIAL AND METHODS

Animals and behavioral testing

All procedures were approved by the Animal Care Committee at The Hospital for Sick Children (protocol #65769) and conducted in compliance with guidelines from the Canadian Council on Animal Care. Homozygous Ai32 mice (Jax #012569), which express ChR2(H134R)-eYFP in a Cre-dependent manner, were crossed with either $Na_V1.8$-Cre mice (Tg(Scn10a-cre)1Rkun) provided by Rohini Kuner to generate mice that express ChR2 in nociceptive afferents (55), or with advillin-Cre mice provided by Fan Wang (equivalent to Jax #032536) to generate mice that express ChR2 in all afferents (56).

Behavioral experiments were performed on mice of either sex at 8-12 weeks of age. Mice were acclimated to the testing environment for 60 min/day for two days before the testing, and for 60 min prior to each test session. Behavioral tests were conducted using a Reproducible Automated Multimodal algometer, RAMalgo (35). Mice were viewed from below using video. Aiming was controlled by joystick so that the human tester remained distant from the mice. Once initiated by the tester, the testing sequence was entirely automated. The red light, whose reflectance level is used to measure paw withdrawal, was set at 0.3 V with a termination threshold of 0.9. The blue light for optogenetic stimulation was focused to a spot 3.5 mm in diameter, and its intensity was ramped to 0.9 mW/mm^2 (4 V control signal) over 15 s. Light intensity at the target was measured with a s170C photodiode attached to a PM100D optical power meter (Thorlabs). Stimulation stopped automatically when paw withdrawal was detected. Data from each trial were saved to electronic files along with metadata and video. For each test session, each mouse was tested three times; the average withdrawal latency is reported. A test session was conducted at baseline and again 24 and 48 hours after injecting CFA or saline; data from the two post-injection test sessions were averaged. When drug or its vehicle was injected, another test session was conducted starting 30 min after injection.

CFA injection. To induce inflammation, 20 µl of complete Freund's adjuvant (CFA, Sigma, F5881) was injected subdermally into the left hind paw shortly after baseline testing. Mice were lightly anesthetized with isoflurane (3.5%) during injection. Control mice received 20 µl of vehicle, namely phosphate-buffered saline (PBS). Mice were randomly allocated to CFA or saline groups,

but the experimenter was not blinded since automated testing with RAMalgo minimizes the risk of bias.

Drug administration. PF-05089771 (PF-71, 300 nM, Alomone) and PF-01247324 (PF-24, 10 µM, Sigma) were first dissolved in DMSO and then diluted to final concentration with PBS. 20 µl of either drug, both drugs together, or vehicle (DMSO diluted in PBS) was injected subdermally into the left hind paw under light anesthesia with isoflurane. Mice were randomly allocated to drug or vehicle groups.

Acute isolation of dorsal root ganglia (DRG) neurons

DRG neurons were obtained from adult (8-12 week-old) $Na_V1.8$-ChR2 mice as previously described (39). Mice were anesthetized with isoflurane (3.5%) and perfused intracardially with ice-cold HBBS (Ca/Mg free, LifeTech 14170112) supplemented with (in mM) 15 HEPES, 28 Glucose, and 111 sucrose; pH was adjusted with NaOH to 7.3-7.4; osmolarity was 312-319 mOsm. Lumbar DRGs (left L2-5 for naïve mice and L4 only for CFA-injected mice) were collected. After digestion with papain (Worthington Biochemical) and collagenase (Worthington Biochemical)/dispase II (Sigma), DRGs were mechanically triturated, plated onto poly-D lysine-coated coverslips, and incubated in Neurobasal™ media (Gibco 21103-049) supplemented with 1% fetal bovine serum (FBS), B-27™ supplement (Thermo Fisher 17504-044) and 0.5 mM L-Glutamine (Gibco 25030-081) for 2 hours. After this, fresh media was added to the wells after removal of unattached cells and cells were maintained in a 5% CO_2 incubator at 37°C until recording.

Electrophysiological recording

DRG neurons were tested 2-8 h after plating to avoids changes in nociceptor excitability (39) and ChR2 expression (11) reported to occur after culturing. Coverslips were transferred to a recording chamber perfused with oxygenated (5% CO_2:95% O_2) artificial cerebrospinal fluid containing (in mM) 126 NaCl, 2 KCl, 2 $CaCl_2$, 1.25 NaH_2PO_4, 26 $NaHCO_3$, 2 $MgCl_2$, and 10 glucose at room temperature. Neurons were visualized with a Zeiss AxioExaminer microscope with a 40x, 0.75 NA water immersion objective (N-Achroplan, Zeiss) and IR-1000 Infrared CCD camera (Dage-MTI). A blue LED (Thorlabs, M455L4) was attached to the epifluorescent port through a collimator; this is the same LED used on RAMalgo. A long-pass filter (OG590) was placed in the transmitted light path to prevent unintended ChR2 activation during recording. Small neurons (diameter <25 µm)

expressing YFP were targeted for patching. Whole cell patch clamp recordings were performed using a pipette solution containing (in mM) 140 K-gluconate, 2 $MgCl_2$, 10 HEPES, 0.2 EGTA, 3.8 Na-ATP, and 0.4 Na-GTP (pH ~7.3, osmolarity ~300 mOsm). Series resistance was compensated >70%. Signals were amplified with an Axopatch 200B amplifier (Molecular Device), low-pass filtered at 2 kHz, digitized with a Power1401 DAQ (Cambridge Electric Design, CED), and recorded at 10 kHz using Signal v7 (CED). All reported voltages are corrected for junction potential (-15 mV).

After determining resting membrane potential, voltage was adjusted to -70 mV to characterize excitability. Spikes were evoked by a series of 1-s-long depolarizing current steps. Rheobase, defined as the minimal current required to evoke a spike, was determined and current steps were then applied at 0.5x increments of rheobase. Firing >2 spikes in response to any stimulus intensity qualifies a neuron as repetitive spiking; transient spiking is defined as consistently firing $\leq$2 spikes. Spike threshold was defined as voltage where dV/dt exceeds 5 mV/ms. Optogenetic stimuli were applied in two ways. To measure ChR2 current, the neuron was voltage clamped at -70 mV while applying blue light as either a series of 1 s-long steps incremented at 0.2 V (max 2 V) or a 15 s-long ramp (max 4 V). The latter stimulus was also applied in current clamp to characterize optogenetically evoked spiking. Light intensity at the neuron was measured using a s170C photodiode attached to a PM100D optical power meter (Thorlabs); 1 V = 78 mW/mm^2

Statistical analysis

Data were analysed with SigmaPlot 11 (SYSTAT). Normality of distributions was tested with the Shapiro-Wilk test. Data are summarized as mean ± SEM or as median, interquartile range (IQR, i.e. 25th-75th percentile) for normally and non-normally distributed data, respectively. Box-and-whisker plots show the median (thick bar), IQR (gray box), and 5th-95th percentile (whiskers). Appropriate parametric or non-parametric tests were applied. Tests and degrees of freedom are identified when reporting results. Effect size was quantified as Hedges' *g*, which is Cohen's *d* (the difference in means divided by pooled standard deviation) corrected for different sample sizes.

REFERENCES

1. K. Deisseroth, Optogenetics. *Nat Methods* **8**, 26-29 (2011).
2. A. M. Packer, B. Roska, M. Hausser, Targeting neurons and photons for optogenetics. *Nat Neurosci* **16**, 805-815 (2013).
3. J. H. Marshel, T. Mori, K. J. Nielsen, E. M. Callaway, Targeting single neuronal networks for gene expression and cell labeling in vivo. *Neuron* **67**, 562-574 (2010).
4. L. Sjulson, D. Cassataro, S. DasGupta, G. Miesenböck, Cell-specific targeting of genetically encoded tools for neuroscience. *Annu Rev Genet* **50**, 571-594 (2016).
5. C. K. Kim, A. Adhikari, K. Deisseroth, Integration of optogenetics with complementary methodologies in systems neuroscience. *Nat Rev Neurosci* **18**, 222-235 (2017).
6. S. Dufour, Y. De Koninck, Optrodes for combined optogenetics and electrophysiology in live animals. *Neurophotonics* **2**, 031205 (2015).
7. N. C. Pégard *et al.*, Three-dimensional scanless holographic optogenetics with temporal focusing (3D-SHOT). *Nature communications* **8**, 1228 (2017).
8. J. A. Cardin *et al.*, Targeted optogenetic stimulation and recording of neurons in vivo using cell-type-specific expression of Channelrhodopsin-2. *Nat Protoc* **5**, 247-254 (2010).
9. M. Izquierdo-Serra, J. J. Hirtz, B. Shababo, R. Yuste, Two-photon optogenetic mapping of excitatory synaptic connectivity and strength. *iScience* **8**, 15-28 (2018).
10. J. Mattis *et al.*, Principles for applying optogenetic tools derived from direct comparative analysis of microbial opsins. *Nat Methods* **9**, 159-172 (2012).
11. Y. Zhu, B. Feng, E. S. Schwartz, G. F. Gebhart, S. A. Prescott, Novel method to assess axonal excitability using channelrhodopsin-based photoactivation. *J Neurophysiol* **113**, 2242-2249 (2015).
12. C. M. Lewis *et al.*, Cortical gamma-band resonance preferentially transmits coherent input. *Cell Rep* **35**, 109083 (2021).
13. D. Usoskin *et al.*, Unbiased classification of sensory neuron types by large-scale single-cell RNA sequencing. *Nat Neurosci* **18**, 145-153 (2015).
14. S. A. Prescott, S. Ratté, Pain processing by spinal microcircuits: afferent combinatorics. *Curr Opin Neurobiol* **22**, 631-639 (2012).
15. S. A. Prescott, Q. Ma, Y. De Koninck, Normal and abnormal coding of somatosensory stimuli causing pain. *Nat Neurosci* **17**, 183-191 (2014).
16. R. Melzack, P. D. Wall, Pain mechanisms: a new theory. *Science* **150**, 971-979 (1965).
17. B. A. Copits, M. Y. Pullen, R. W. Gereau, Spotlight on pain: optogenetic approaches for interrogating somatosensory circuits. *Pain* **157**, 2424-2433 (2016).
18. Y. F. Xie, J. Wang, R. P. Bonin, Optogenetic exploration and modulation of pain processing. *Exp Neurol* **306**, 117-121 (2018).
19. S. Maksimovic *et al.*, Epidermal Merkel cells are mechanosensory cells that tune mammalian touch receptors. *Nature* **509**, 617-621 (2014).
20. A. Arcourt *et al.*, Touch receptor-derived sensory information alleviates acute pain signaling and fine-tunes nociceptive reflex coordination. *Neuron* **93**, 179-193 (2017).

21. L. E. Browne *et al.*, Time-resolved fast mammalian behavior reveals the complexity of protective pain responses. *Cell Rep* **20**, 89-98 (2017).
22. R. Dhandapani *et al.*, Control of mechanical pain hypersensitivity in mice through ligand-targeted photoablation of TrkB-positive sensory neurons. *Nat Com* **9**, 1640 (2018).
23. A. Chamessian *et al.*, Is Optogenetic activation of Vglut1-positive Abeta low-threshold mechanoreceptors sufficient to induce tactile allodynia in mice after nerve injury? *J Neurosci* **39**, 6202-6215 (2019).
24. C. Warwick *et al.*, Mrgprd-Cre lineage neurons mediate optogenetic allodynia through an emergent polysynaptic circuit. *Pain* **162**, 2120-2131 (2021).
25. H. Beaudry, I. Daou, A. R. Ase, A. Ribeiro-da-Silva, P. Seguela, Distinct behavioral responses evoked by selective optogenetic stimulation of the major TRPV1+ and MrgD+ subsets of C-fibers. *Pain* **158**, 2329-2339 (2017).
26. A. Schorscher-Petcu, F. Takács, L. E. Browne, Scanned optogenetic control of mammalian somatosensory input to map input-specific behavioral outputs. *Elife* **10**, 62026 (2021).
27. I. Daou *et al.*, Remote optogenetic activation and sensitization of pain pathways in freely moving mice. *J Neurosci* **33**, 18631-18640 (2013).
28. S. M. Iyer *et al.*, Virally mediated optogenetic excitation and inhibition of pain in freely moving nontransgenic mice. *Nat Biotechnol* **32**, 274-278 (2014).
29. H. Abdo *et al.*, Specialized cutaneous Schwann cells initiate pain sensation. *Science* **365**, 695-699 (2019).
30. A. Barik, J. H. Thompson, M. Seltzer, N. Ghitani, A. T. Chesler, A brainstem-spinal circuit controlling nocifensive behavior. *Neuron* **100**, 1491-1503.e1493 (2018).
31. B. Sharif, A. R. Ase, A. Ribeiro-da-Silva, P. Seguela, Differential coding of itch and pain by a subpopulation of primary afferent neurons. *Neuron* **106**, 940-951 (2020).
32. R. Tashima *et al.*, Optogenetic activation of non-nociceptive Abeta fibers induces neuropathic pain-like sensory and emotional behaviors after nerve injury in rats. *eNeuro* **5**, e0450-0417.2018 (2018).
33. T. Maruta *et al.*, Comparison of nocifensive behavior in Nav1.7-, Nav1.8-, and Nav1.9-channelrhodopsin-2 mice by selective optogenetic activation of targeted sodium channel subtype-expressing afferents. *J Neurosci Res* **102**, e25386 (2024).
34. T. Maruta *et al.*, Selective optogenetic activation of Nav1.7-expressing afferents in Nav1.7-ChR2 mice induces nocifensive behavior without affecting responses to mechanical and thermal stimuli. *PLoS One* **17**, e0275751 (2022).
35. C. Dedek, M. A. Azadgoleh, S. A. Prescott, Reproducible and fully automated testing of nocifensive behavior in mice. *Cell Rep Methods* **3**, 100650 (2023).
36. J. L. Hurst, R. S. West, Taming anxiety in laboratory mice. *Nat Methods* **7**, 825-826 (2010).
37. L. Djouhri *et al.*, The TTX-resistant sodium channel Nav1.8 (SNS/PN3): expression and correlation with membrane properties in rat nociceptive primary afferent neurons. *J Physiol* **550**, 739-752 (2003).
38. L. Djouhri *et al.*, Sensory and electrophysiological properties of guinea-pig sensory neurones expressing Nav1.7 (PN1) Na+ channel alpha subunit protein. *J Physiol* **546**, 565-576 (2003).

39. Y. F. Xie, J. Yang, S. Ratté, S. A. Prescott, Similar excitability through different sodium channels and implications for the analgesic efficacy of selective drugs. *Elife* **12**, 90960 (2024).
40. L. Djouhri, S. N. Lawson, Changes in somatic action potential shape in guinea-pig nociceptive primary afferent neurones during inflammation in vivo. *J.Physiol* **520**, 565-576 (1999).
41. S. Ratté, M. Lankarany, Y. A. Rho, A. Patterson, S. A. Prescott, Subthreshold membrane currents confer distinct tuning properties that enable neurons to encode the integral or derivative of their input. *Front Cell Neurosci* **8**, 452 (2015).
42. S. A. Prescott, Y. De Koninck, T. J. Sejnowski, Biophysical basis for three distinct dynamical mechanisms of action potential initiation. *PLoS Comput.Biol.* **4**, e1000198 (2008).
43. E. J. Chesler, S. G. Wilson, W. R. Lariviere, S. L. Rodriguez-Zas, J. S. Mogil, Influences of laboratory environment on behavior. *Nat Neurosci* **5**, 1101-1102 (2002).
44. S. R. Chaplan, F. W. Bach, J. W. Pogrel, J. M. Chung, T. L. Yaksh, Quantitative assessment of tactile allodynia in the rat paw. *J Neurosci Methods* **53**, 55-63 (1994).
45. D. Le Bars, M. Gozariu, S. W. Cadden, Animal models of nociception. *Pharmacol Rev* **53**, 597-652 (2001).
46. B. Sagalajev *et al.*, Absence of paresthesia during high-rate spinal cord stimulation reveals importance of synchrony for sensations evoked by electrical stimulation. *Neuron* **112**, 404-420.e406 (2024).
47. R. R. Ji, Z. Z. Xu, Y. J. Gao, Emerging targets in neuroinflammation-driven chronic pain. *Nat Rev Drug Discov* **13**, 533-548 (2014).
48. M. S. Gold, G. F. Gebhart, Nociceptor sensitization in pain pathogenesis. *Nat Med* **16**, 1248-1257 (2010).
49. S. G. Waxman, G. W. Zamponi, Regulating excitability of peripheral afferents: emerging ion channel targets. *Nat Neurosci* **17**, 153-163 (2014).
50. Y. A. Rho, S. A. Prescott, Identification of molecular pathologies sufficient to cause neuropathic excitability in primary somatosensory afferents using dynamical systems theory. *PLoS Comput Biol* **8**, e1002524 (2012).
51. S. Ratté, Y. Zhu, K. Y. Lee, S. A. Prescott, Criticality and degeneracy in injury-induced changes in primary afferent excitability and the implications for neuropathic pain. *eLife* **3**, 02370 (2014).
52. S. Ratté, S. A. Prescott, Afferent hyperexcitability in neuropathic pain and the inconvenient truth about its degeneracy. *Curr Opin Neurobiol* **36**, 31-37 (2016).
53. C. Wong *et al.*, mTORC2 mediates structural plasticity in distal nociceptive endings that contributes to pain hypersensitivity following inflammation. *J Clin Invest* **132** (2022).
54. S. Tyagi *et al.*, Compartment-specific regulation of Nav1.7 in sensory neurons after acute exposure to TNF-α. *Cell Rep* **43**, 113685 (2024).
55. N. Agarwal, S. Offermanns, R. Kuner, Conditional gene deletion in primary nociceptive neurons of trigeminal ganglia and dorsal root ganglia. *Genesis* **38**, 122-129 (2004).
56. X. Zhou *et al.*, Deletion of PIK3C3/Vps34 in sensory neurons causes rapid neurodegeneration by disrupting the endosomal but not the autophagic pathway. *Proc Natl Acad Sci U S A* **107**, 9424-9429 (2010).

FIGURE LEGENDS

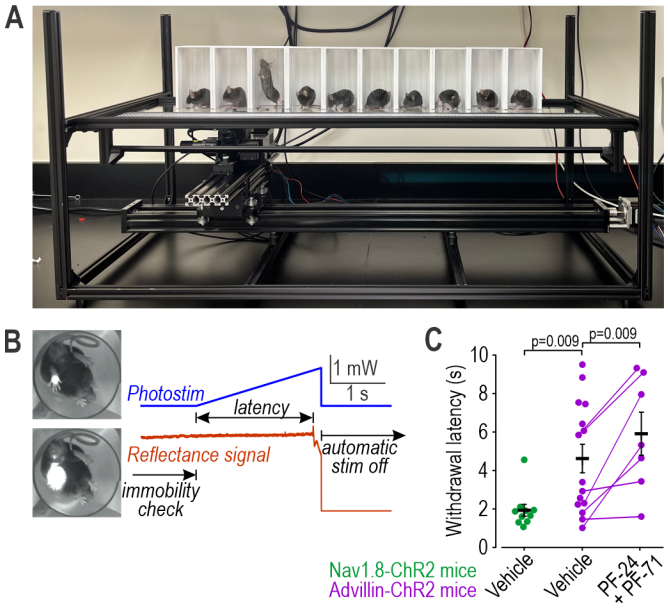

FIGURE 1. Responses to transcutaneous optogenetic activation of different subsets of afferents

(A) RAMalgo with 10 mice on the testing platform. The stimulator is located below the platform, mounted on linear actuators for joystick-controlled aiming. Components for mechanical stimulation are removed to give a clearer view of photostimulation components. Mice undergo one trial each in rapid succession before starting a second round of trials, thus ensuring each mouse has a long inter-stimulus interval while minimizing the total time taken to test all mice.

(B) Sample trial showing photostimulus (blue, top) and red reflectance signal (red, bottom) for a Nav1.8-ChR2 mouse tested at baseline; see Video 1 for full response. Blue photostimulation is initiated if the paw is deemed immobile (based on stability of the reflectance signal) during the pre-stimulus period. Abrupt changes in the reflectance signal caused by paw withdrawal are used to automatically measure withdrawal latency and terminate stimulation. Photos show frames captured from video. The blue photostimulus is restricted to a spot centered on the paw (top) and is shown here separately for illustrative purposes, as it is usually subsumed within the larger area of red illumination (bottom).

(C) Withdrawals evoked by selectively activating nociceptors in $Na_V1.8$-ChR2 mice (green, 1.926 ± 0.309 s, mean ± SEM) were significantly faster than withdrawals evoked by co-activating all somatosensory afferents in advillin-ChR2 mice (purple, 4.614 ± 0.742 s) (T_{23} = -2.83, p = 0.009, unpaired t-test). Both data sets are based on responses measured >30 min after injecting vehicle. On a separate day, a subset of advillin-ChR2 mice were injected with PF-24 and PF-71 to silence nociceptors, which delayed withdrawal by 2.853 ± 0.744 s (T_6 = -3.836, p = 0.009, paired t-test).

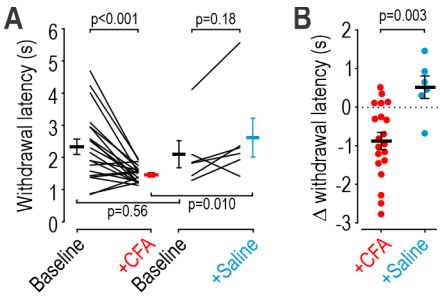

FIGURE 2. Effects of CFA on paw withdrawal from transcutaneous optogenetic stimulation.

(A) Withdrawal latency is plotted for each Nav1.8-ChR2 mouse at baseline and again after injecting CFA (left) or saline (right). Treatment (CFA vs saline) interacted significantly with time (baseline vs. post-injection) ($F_{1,24}$ = 10.914, p = 0.003, two-way repeated measures ANOVA). Withdrawal latency (mean ± SEM) differed between CFA and saline conditions post-injection (1.472 ± 0.058 s vs 2.616 ± 0.606 s, p = 0.010, Student-Neuman-Keuls post-hoc test) but not at baseline (2.345 ± 0.239 s vs 2.097 ± 0.420 s, p = 0.56).

(B) Change in latency due to treatment calculated within each mouse. The reduction in withdrawal latency due to CFA (red, -0.873 ± 0.212 s) differed significantly from the increase due to saline (blue, 0.519 ± 0.291 s) (T_{24} = -3.304, p = 0.003, unpaired t-test).

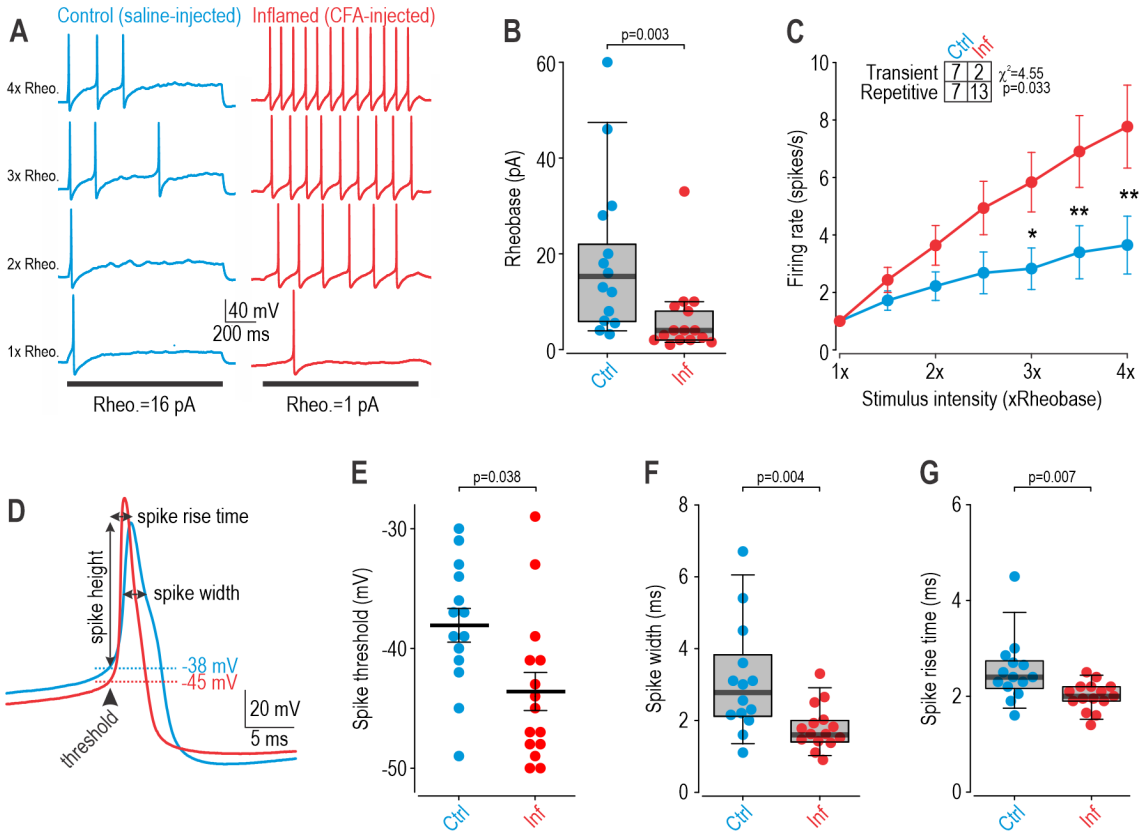

FIGURE 3. Effects of CFA on the somatic excitability of nociceptors.

(A) Sample current clamp recordings show spiking evoked by current injection in a typical control (blue) and inflamed (red) neuron. Rheobase was determined for each neuron as the weakest current step required to evoke a spike. Current injection was incremented as multiples of rheobase for each neuron. Inflamed neurons responded vigorously even to weak stimulation.

(B) Rheobase was significantly lower in inflamed neurons (4, 2 – 8.75 pA; median, IQR) than in control neurons (14.5, 6 – 28 pA) (U_{27} = 36, p = 0.003, Mann-Whitney U-test).

(C) Evoked firing rates depended jointly on stimulus intensity and condition (interaction, $F_{6,168}$ = 4.834, p < 0.001, two-way repeated measures ANOVA). Results of post-hoc Student-Neuman-Keuls tests are summarized on graph (*, p < 0.05; **, p < 0.01). Weaker stimuli were applied to inflamed neurons than to control neurons because of the difference in rheobase, meaning an even a larger inflammation-induced increase in evoked firing would be seen if absolute stimulus intensities was matched. Table shows that transient spiking neurons (i.e. neurons that never fire >2 spikes during current injection) are significantly less common after inflammation than in control conditions (χ^2 = 4.55, p = 0.033).

(D) Enlarged traces highlight differences in spike waveform. Arrows show measurements compared in panels E-G. The first spike evoked by rheobasic stimulation was measured.

(E) Spike threshold was significantly more negative in inflamed neurons (-43.6 ± 1.6 mV) than in control neurons (-38.1 ± 1.4 mV) (T_{27} = 2.58, p = 0.016, unpaired t-test). Threshold was defined as the voltage where dV/dt exceeds 5 mV/ms

(F) Spikes were significantly narrower in inflamed neurons (1.6, 1.413 – 1.975 ms) than in control neurons (2.775, 2.15 – 3.6 ms) (U_{27} = 39, p = 0.004). Width was measured at half of the spike height.

(G) Spikes rose significantly faster in inflamed neurons (2.0, 1.9 – 2.2 ms) than in control neurons (2.4, 2.2 – 2.7 ms) (U_{27} = 42.5, p = 0.007). Rise time was measured from threshold crossing to peak voltage.

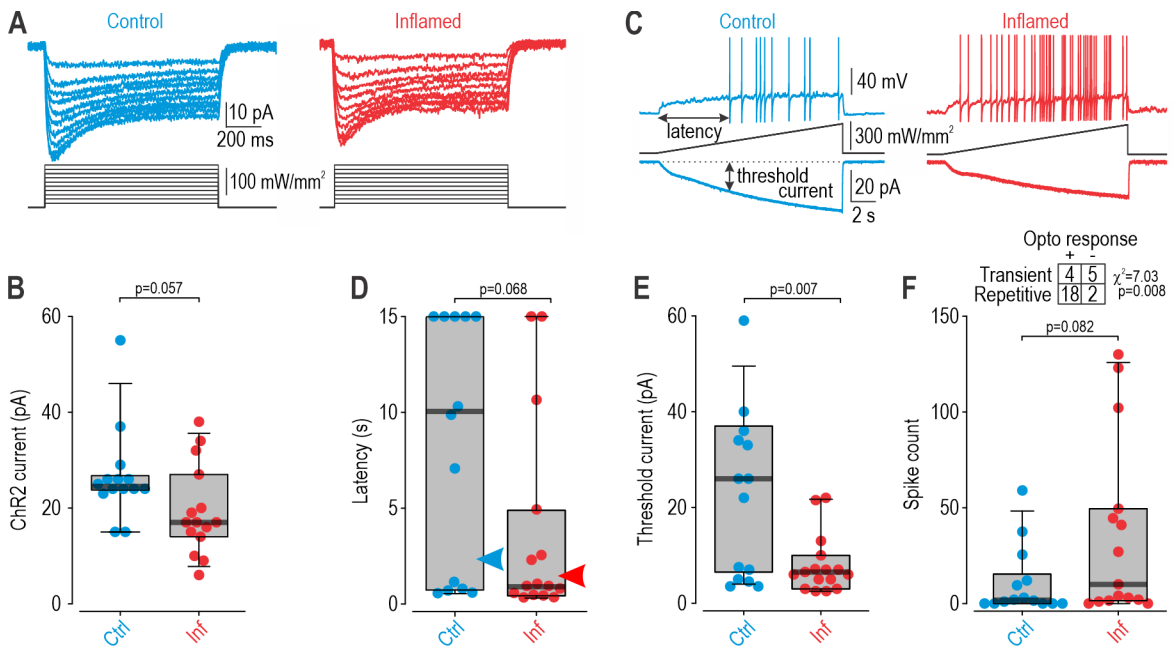

FIGURE 4. Effects of CFA on ChR2-expression and optogenetically evoked somatic spiking.

The same neurons characterized in Figure 3 were tested optogenetically in Figure 4.

(A) Sample voltage clamp recordings show current evoked by optogenetic stimulation with blue light applied as 1 s-long step at different intensities to a typical control (blue) and inflamed (red) neuron. No differences in ChR2 gating kinetics were observed.

(B) ChR2 current evoked by 156 mW/mm^2 blue light in inflamed neurons (17, 14.25 – 25.25 pA) was slightly smaller than in control neurons (24.5, 24 – 26 pA) but the difference did not reach significance (U_{27} = 61, p = 0.057).

(C) Sample current clamp recordings (top) show spiking evoked by a 15-s-long optogenetic ramp. Bottom traces show ChR2 current evoked by the equivalent optogenetic ramp applied during voltage clamp. Arrows highlight measurements compared in panels D-F. Sample traces in C are from the same neurons illustrated in panel A. Spiking was increased in inflamed neuron because of increased excitability, despite reduced ChR2 current.

(D) Latency to the first spike was significantly shorter in inflamed neurons (0.940, 0.489-4.330 s) than in control neurons (10.085, 0.785 – 15 s) (U_{27} = 64, p = 0.068). Neurons that did not respond with any spikes were treated as having a latency of 15 s. Arrowheads mark average withdrawal latency for the respective condition (see Fig. 2A).

(E) Threshold current (i.e. ChR2 current at the time of the first spike) was significantly lower in inflamed neurons (6.5, 3.5 – 9.275 pA) than in control neurons (26, 7 – 36 pA) (U_{27} = 42.5, p = 0.007).

(F) The number of optogenetically evoked spikes in inflamed neurons (10, 1.625 – 48.25 spikes) was higher than in control neurons (1.75, 0 – 12 spikes), but the difference did not reach significance (U_{27} = 65, p = 0.082). Table shows that repetitive spiking neurons are significantly more likely than transient spiking neurons to respond to the optogenetic ramp with at least one spike (χ^2 = 7.03, p = 0.008), which is notable given the shift from transient to repetitive spiking after inflammation (see table on Fig.3C).

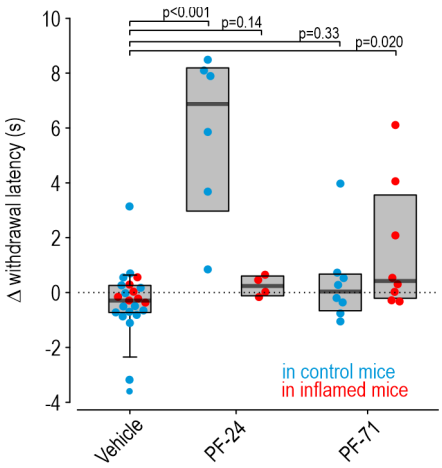

FIGURE 5. Differential effects of subunit-selective Na_V inhibitors on withdrawal confirm that axons experience an inflammation-induced shift from $Na_V1.8$ to $Na_V1.7$.

Data are plotted as the change in withdrawal latency induced by injecting drug or vehicle into the optogenetically stimulated paw. Injecting vehicle had an equivalent effect in control and inflamed mice (U_{21} = 34, p = 0.15, Mann-Whitney U test) and data were therefore pooled to give a median latency change of -0.290, -0.722 – 0.239 s. The effect of blocking $Na_V1.8$ or $Na_V1.7$ with PF-24 and PF-71, respectively, are compared against the vehicle effect. PF-24 significantly increase withdrawal latency by 6.871, 3.676 – 8.096 s in control mice (U_{27} = 1, p < 0.001) but caused only a 0.239, -0.073 – 0.552 s increase in inflamed mice (U_{25} = 24, p = 0.14). Conversely, PF-71 increased withdrawal latency by only 0.039, -0.564 – 0.624 s in control mice (U_{29} = 70, p = 0.33) but significantly increased it by 0.417, -0.133 – 3.066 s in inflamed mice (U_{29} = 40, p = 0.020).

SUPPLEMENTAL VIDEOS

Video 1. Sample response to ramped optogenetic stimulation in a naïve $Na_V1.8$-ChR2 mouse. Inset shows the temporal evolution of the blue photostimulus and red reflectance signal synced to the video. Notice the drop in reflectance coincident with paw withdrawal. The relatively small area of blue photostimulation is not discernable inside the larger area of red illumination.

Video 2. Lack of response to ramped optogenetic stimulation in a ChR2-negative mouse. The absence of response confirms that blue photostimulation is not intrinsically painful, and nor does the photostimulus seem to draw visual attention. Mice cannot see the red light used for reflectance measurements.

Video 3. Sample response to ramped optogenetic stimulation in the same $Na_V1.8$-ChR2 mouse shown in Video 1, but now one day after it received CFA in the stimulated paw.